Adsorption of DNA onto positively charged amidine colloidal spheres and the resultant bridging interaction

Alison J. Hodrien [a], Thomas A. Waigh [b,*], Alison M. Voice [a],
G. Eric Blair [c], Stuart M. Clarke [d]

[a] *Polymers and Complex Fluids, Department of Physics and Astronomy, University of Leeds, Leeds, West Yorkshire LS2 9JT, UK*
[b] *Biological Physics, Department of Physics and Astronomy, University of Manchester, PO Box 88, Sackville Street, M60 1QD, UK*
[c] *School of Biochemistry and Microbiology, University of Leeds, Leeds, West Yorkshire LS2 9JT, UK*
[d] *Department of Chemistry, University of Cambridge, Lensfield Road, Cambridge CB2 1EW, UK*

Abstract

The complexation behaviour of duplex linear DNA (negatively charged) with amidine functionalised sub-micron latex spheres (positively charged) was studied using dynamic light scattering (DLS) and a PALS interferrometric zeta potential sizer. Four types of DNA-sphere complex were investigated as a function of component concentration by combining amidine functionalised polystyrene microspheres with radii of 10.5 nm and 60 nm, and herring DNA of lengths of 35 nm and 85 nm. At low DNA concentrations (c_{DNA}), the *undercharged* complexes showed a small increase in measured hydrodynamic radius (R_h) and a decrease in zeta potential with increasing c_{DNA}. Within a critical DNA concentration range R_h was seen to peak sharply, and the zeta potentials were ∼0 mV, corresponding to the formation of unstable neutral complexes. Immediately above this concentration region the measured R_h values became comparable with those at low c_{DNA}, and the zeta potential became negative, indicating the formation of stable *overcharged* complexes. The small and large spheres formed multi-sphere and single sphere *overcharged* aggregates respectively, which is thought to be determined by the relative magnitude of the chain persistence length (∼50 nm) and the sphere radius, switching on or off the DNA *bridging interaction*.
© 2007 Published by Elsevier B.V.

Keywords: DNA; Colloid; Amidine; Complexation; DLS; Zeta potential; Overcharged; Polyelectrolyte bridging

1. Introduction

The phenomenon of complexation between oppositely charged nanostructures is exploited by man and nature, e.g. industrially for colloidal stabilisation, and biologically for DNA packaging within cells. Motivation for the current work stems from the growing body of theoretical literature on the subject of polyelectrolyte complexation, which currently lacks an equivalent body of experimental work for the purposes of comparison and validation. The existing theoretical literature describes a range of structures for sphere-chain complexes. The chains can be tightly wrapped around the sphere or adopt extended conformations, with large loops (or leaves) giving a rosette like structure [1–3]. For simplicity, the key parameters inves-

tigated in the present study were the sphere radius and the chain length.

The experimental system chosen is compared with theoretical works based on complexation between a charged semi-flexible chain and an oppositely charged sphere. By varying parameters, such as the relative component size, different behaviours for the system are expected [1–3]. The transition from large to small spheres corresponds to a change from a locally flat surface to a highly curved one leading to a series of fundamental changes in the physics of complexation, due to the magnitude of the bending energy of the DNA (related to its persistence length) relative to the adsorption energy [1–3] and the nature of counterion condensation [4–6].

An area of current importance for the polymer physics of DNA is that of drug delivery. The medical profession increasingly desire the ability to deliver drugs to a specific organ or area of the body; the "magic bullet" approach. This can be useful to reduce the size of dose that needs to be administered (reducing

* Corresponding author. Tel.: +44 161 306 8881; fax: +44 161 306 3941.
E-mail address: t.a.waigh@manchester.ac.uk (T.A. Waigh).

both costs and side effects), or to reduce damage to healthy tissues due to the drug's toxicity. This kind of treatment is appropriate for cancers, where anti-tumour drugs could be delivered specifically to the tumour site [7], and cystic fibrosis where it is hoped that genetic material can be delivered to compensate for a mutant gene in the epithelia lining of the lungs [8]. One particularly effective strategy being investigated is the use of carrier particles to house drugs while in vivo. Viruses have been investigated for this purpose, but are not always suited to a specific target, and have in some trials provoked a fatal immune response. To try and circumvent these problems, special biocompatible molecules are being designed which will carry drug molecules either within their core or attached to their surface to a desired target [9,10]. There are many considerations involved in their synthesis: bio-compatibility of components, interaction with white blood cells, the need for functional groups that will bond to a specific organ or tissue type to help the molecule reach its target. Also, in the case of gene therapy the DNA to be delivered needs to be in a collapsed state so that it is compact enough (and suitably charged) to pass through a cell membrane. The physics of a non-specific self-assembled mechanism for electrostatic compaction and complexation is considered in the present article.

A comprehensive review of the physics of DNA complexation has recently been completed [11]. Advances relevant to the current work include the experimental demonstration of a cascade of first order binding transitions between long DNA chains and small oppositely charged colloidal particles [12], and the prediction of nearly neutral or undercharged complexes in simulations [13]. The role of polyelectrolyte bridging interactions on colloidal stability has also been highlighted in a recent review [14].

Dynamic light scattering (DLS) and zeta potential measurements are both high resolution non-invasive techniques that can be used to characterise submicron particles in suspension. The former is used to measure the rate of diffusion of particles in order to ascertain particle size, while the latter is used to measure the zeta potential of the particles. Unlike some other scattering techniques (X-ray scattering and electron microscopy), dynamic light scattering does not damage biological samples and has a vast range of operating time scales (12.5 ns–1000 s). Zeta potential measurements in aqueous solutions have recently experienced an order of magnitude increase in sensitivity due to the introduction of the PALS interferometric method of detection allowing accurate measurement of nm sized particles [15]. In this work, DLS and zeta potential techniques were used to characterize amidine functionalised microspheres with and without an adsorbed layer of DNA, as a function of DNA concentration.

2. Experimental

2.1. Materials

Amidine functionalised polystyrene microspheres with radii of 60 nm and 10.5 nm were purchased from Interfacial Dynamics Corporation (Portland, Oregon, U.S.A.), and were received suspended in distilled deionised water at 4% solids. The charge on the spheres obtained by conduction titrations were 8.1 μC/cm^2 and 2.9 μC/cm^2 for the 60 nm and 10.5 nm spheres respectively which correspond to $(23.7)^2$ Å^2 and $(14.1)^2$ Å^2 per positively charged group. Thus a small amount of random patchiness is possible at the 1 nm length scale, but it is not expected at the coarse grained level of the whole colloid. Double stranded DNA extracted from herring testes was purchased from Sigma–Aldrich (product number D-6898) and was received as a lyophilized powder. Gel electrophoresis showed that the two batches received were relatively pure but had different sizes. The sizes of the two DNA samples were 100 base pairs (100 bp, 35 nm contour length) and 250 base pairs (250 bp, 85 nm contour length). Furthermore a small number of experiments were performed with linear duplex plasmid DNA (3400 bp). The size designations were in agreement with DLS measurements on dilute DNA in high salt conditions (DNA polydispersities were found to be $\pm 2\%$) and intrinsic viscosity measurements with video particle tracking microrheology.

2.2. Sample preparation

As the amidine groups on the spheres were extremely sensitive to the aggregating effects of multivalent anions, samples were made with analytical grade water from a Millipore system using plastic volumetric ware and storage containers. Dilute stock solutions of the four components were prepared. The complexes were assembled by combining the DNA, spheres and water in varying volumes to provide samples at the required concentrations. The sphere concentration was kept constant (at 100 μg/ml for the 10.5 nm radius spheres and at 25 μg/ml for the 60 nm radius spheres) while the DNA concentration was varied. Samples for zeta potential measurements were prepared at 5 mM NaCl in order to provide a constant ionic strength. After mixing, samples were shaken for a minimum of 12 h at $\sim$25 $^\circ$C. DNA, spheres, stock solutions and the assembled complexes were all stored at 4 $^\circ$C.

2.3. Methods

DLS measurements were made using an ALV-5000 compact goniometer system (ALV-GmbH, Langen, Germany) with the sample illuminated with a 488 nm wavelength Spectra-Physics 2016 Ar$^+$ laser (Spectra-Physics Laser Division, CA, U.S.A.). The temperature control was provided by the toluene bath surrounding the sample cuvette and was maintained at 25.0 $\pm$ 0.1 $^\circ$C. Correlation functions were collected at scattering angles between 30° and 140° with an angular step of 10°. The collection time at each angle was between 5 and 10 min depending on the signal to noise ratio.

Zeta potential measurements were made using a Zetasizer Nano ZS (Malvern Instruments, Malvern, UK). The temperature was again maintained at 25 $^\circ$C. A 0.75 ml of sample was contained in a disposable folded capillary cell with integral electrodes. Each measurement consisted of a minimum of 20 runs, and three measurements were made on each sample allowing anomalous results to be identified and discarded. Zeta potential

distributions were determined automatically by the accompanying software, along with the peak position, width and area. Up to three peaks could be identified in each case.

2.4. Analysis of DLS data

Dynamic light scattering experiments measure the intensity correlation function ($g_2(\tau)$) of light scattered from a sample [16]:

$$g_2(\tau) = \frac{\langle I_t I_{t+\tau} \rangle}{\langle I_t \rangle^2} \tag{1}$$

where I_t is the intensity of scattered light at time t and $I_{t+\tau}$ is the intensity of scattered light after the delay time, τ. The intensity correlation function can be expressed in terms of the field correlation function ($g_1(\tau)$) via the Siegert relation (for an optical field obeying Gaussian statistics):

$$g_2(\tau) = 1 + |g_1(\tau)|^2 \tag{2}$$

Standard CONTIN analysis of the intensity correlation curves showed either a monomodal or bimodal decay rate distribution. In the case of clearly monomodal distributions, the diffusion coefficient (D) was determined from the peak position, which indicates the characteristic decay time, τ_c:

$$\Gamma = Dq^2 = \frac{1}{\tau_c} \tag{3}$$

where q is the wavevector defined as $q = (4\pi n_0/\lambda) \sin(\theta/2)$, with the scattering angle θ, wavelength of scattered light λ and solvent refractive index n_0.

For bimodal distributions, or monomodal distributions that were suggestive of bimodal behaviour (e.g. the presence of a shoulder on the peak), a double exponential fit was made to the field correlation function and a pair of diffusion coefficients were determined

$$g_1(\tau) = A_1 \exp(-\Gamma_1 t) + A_2 \exp(-\Gamma_2 t) \tag{4}$$

Diffusion coefficients (D) were subsequently used to calculate the hydrodynamic radii (R_h) of the complexes using the Stokes–Einstein relationship:

$$D = \frac{k_B T}{6\pi\eta_0 R_h} \tag{5}$$

where kT is the thermal energy and η_0 is the viscosity of the solution.

3. Results and discussion

For complexes of 60 nm radius spheres with the two sizes of DNA, DLS measurements were made across a DNA concentration range of 0.005–10 µg/ml (with the sphere concentration held constant at 25 µg/ml). In the case of the 250 bp DNA, CONTIN analysis showed monomodal behaviour for the complexes except in the 0.2–0.6 µg/ml DNA concentration range, where the behaviour was seen to be bimodal and Eq. (4) was used to fit the correlation functions. The results of such fits are shown in Fig. 1.
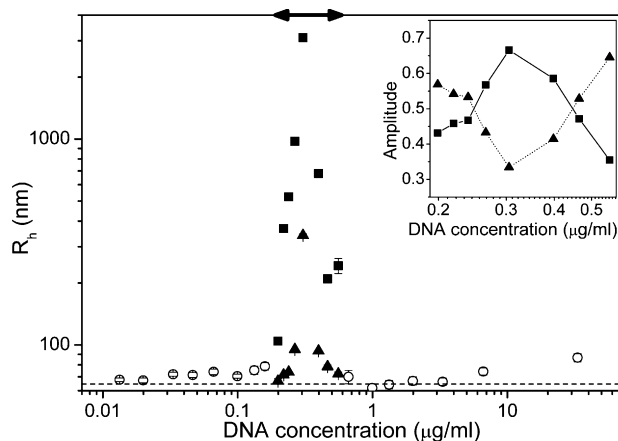

Fig. 1. The hydrodynamic radii (R_h) measured by DLS as a function of DNA concentration for 250 bp DNA complexed with 60 nm radius spheres. Open circles indicate points determined by CONTIN analysis, while solid squares and triangles were obtained from double exponential fits; the relative amplitudes of the solid points are compared in the inset. The dashed line indicates the measured hydrodynamic radius for bare spheres of 64.6 ± 2.3 nm. The continuous arrowed line gives the range of DNA concentrations over which large multi-sphere aggregates formed.

Within this bimodal region of large DNA/sphere complexes, samples prepared at 0.35 µg/ml were repeatedly seen to aggregate and precipitate out of solution, and we were unable to measure accurate values for the hydrodynamic radius. Assuming that all chains within the sample are 250 bp long, this equates to around 50 chains per sphere.

In the bimodal region, the relative amplitudes (A_1 and A_2 in Eq. (4)) were also plotted as a function of concentration (inset, Fig. 1). The amplitude corresponding to the largest hydrodynamic radius peaks at the same DNA concentration as the slow mode amplitude reaches its maximum. This behaviour indicates that as a critical concentration is approached, the complexes in the solution are increasingly incorporated into the large aggregates, but above this concentration the smaller complexes again become more stable and correspondingly increase in number.

Very similar behaviour was seen for the 100 bp DNA complexed with spheres of 60 nm radius, the hydrodynamic radius as a function of DNA concentration for these complexes is shown in Fig. 2.

Again the behaviour of the correlation functions was seen to be monomodal at low and high DNA concentrations, with bimodal behaviour seen in the region 0.04–0.1 µg/ml, which is at a notably lower concentration range than the larger 250 bp DNA. Precipitation out of solution was seen for a sample prepared at 0.08 µg/ml, which assuming that all the chains are 100 bp in length, corresponds to around 30 chains per sphere. For both of the 60 nm sphere complexes, the measured hydrodynamic radius in the monomodal region is slightly larger than that of the bare spheres.

Measurements involving the smaller 10.5 nm radius spheres were more difficult, as they were approaching the limits of the sensitivity of the equipment. Also, because of their lower surface charge density, they are intrinsically less stable to phase separation than their larger counterparts. These small sphere complexes were seen to aggregate over a wider concentration range than the
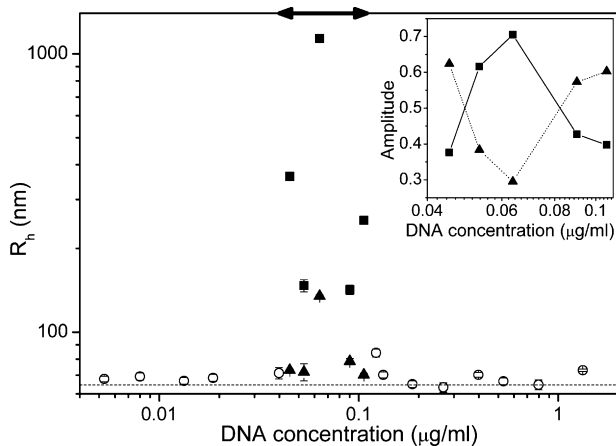
Fig. 2. The hydrodynamic radii (R_h) measured by DLS as a function of DNA concentration for 100 bp DNA complexed with 60 nm radius spheres. Open circles indicate points determined by CONTIN analysis, while solid squares and triangles were obtained from double exponential fits; the relative amplitudes of the solid points are compared in the inset. The dashed line indicates the measured hydrodynamic radius for bare spheres of 64.6 ± 2.3 nm.

larger spheres, and as such only the base of the aggregation peak in the measured hydrodynamic radius is seen (in strong contrast with the relatively sharp peak seen for the larger spheres). For complexes of the 10.5 nm radius spheres with 250 bp DNA, monomodal behaviour was seen below 1 μg/ml and bimodal behaviour across the region 1–50 μg/ml, as in Fig. 3.

Within the bimodal region, measurements could not be made across the range 3–15 μg/ml, as samples precipitated out of solution. The behaviour of the amplitudes of the two modes is different to that seen for the larger radius (60 nm) spheres. As the DNA concentration increases the mode corresponding to larger complexes in the solution dominates. At concentrations above those at which the samples aggregated, the dominant mode corresponds to complexes ∼60 nm in radius, which is significantly larger than the measured bare sphere value of the hydrodynamic
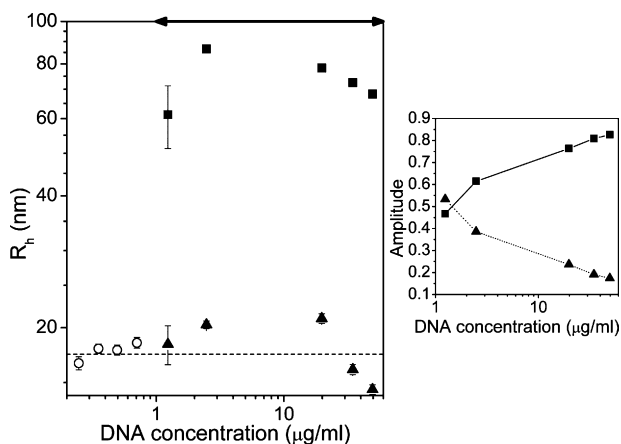
radius 17.4 nm, and shows that these stable complexes contain more than one sphere. For complexes of the 10.5 nm radius spheres with 100 bp DNA, similar behaviour is seen, although only a single sample required the double exponential approach, with all the other samples showing a single mode in the CONTIN analysis, illustrated in Fig. 4.

As with the larger spheres, the range of DNA concentrations over which these small sphere samples aggregated was lower than with the larger 250 bp DNA, in this case the range was 0.6–3 μg/ml. The region of stable complexes at high DNA concentration again have larger hydrodynamic radii than those at low DNA concentration, indicating as for complexes of the 10.5 nm radius spheres with 250 bp DNA that these complexes contain multiple spheres.

Zeta potential measurements were made across concentration ranges comparable to those used in the DLS experiments. A small amount of salt was added to the samples, since the electrophoretic mobility from which the zeta potential was determined has a dependency on the Debye screening length, which is a function of ionic strength. By preparing the samples at a constant ionic strength of 5 mM NaCl, the effect on the ionic strength caused by varying the DNA concentration (and therefore the number of counterions in solution) becomes negligible.

The dependence of the zeta potential of the complexes on the concentration of DNA in solution for samples containing 60 nm radius spheres and 250 bp DNA is shown in Fig. 5.

As the DNA concentration is increased the zeta potential decreases, passing through zero and then reaching a maximum negative zeta potential of approximately −40 mV at a concentration of 0.6 μg/ml, after which point the zeta potential remains constant. These negative zeta potential measurements show that the complexes have become overcharged, meaning that they have adsorbed a sufficient amount of DNA for the net charge of the complex to be opposite in sign to the net charge of the uncomplexed sphere, as indicated by the change in potential.
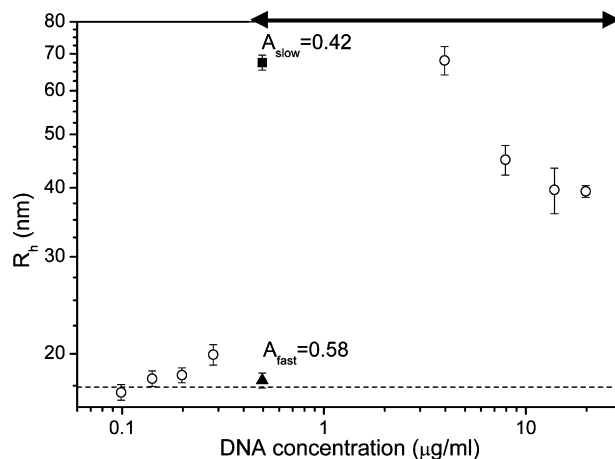

Fig. 3. The hydrodynamic radii (R_h) measured by DLS as a function of DNA concentration for 250 bp DNA complexed with 10.5 nm radius spheres. Open circles indicate points determined by CONTIN analysis, while solid squares and triangles were obtained from double exponential fits; the relative amplitudes of the solid points are compared on the right hand side of the figure. The dashed line indicates the measured hydrodynamic radius for bare spheres of 17.4 ± 0.3 nm.

Fig. 4. The hydrodynamic radii (R_h) measured by DLS as a function of DNA concentration for 100 bp DNA complexed with 10.5 nm radius spheres. Open circles indicate points determined by CONTIN analysis, while the solid square and triangle were obtained from a double exponential fit; the relative amplitudes of the solid points are marked on the figure. The dashed line indicates the measured hydrodynamic radius for bare spheres of 17.4 ± 0.3 nm.
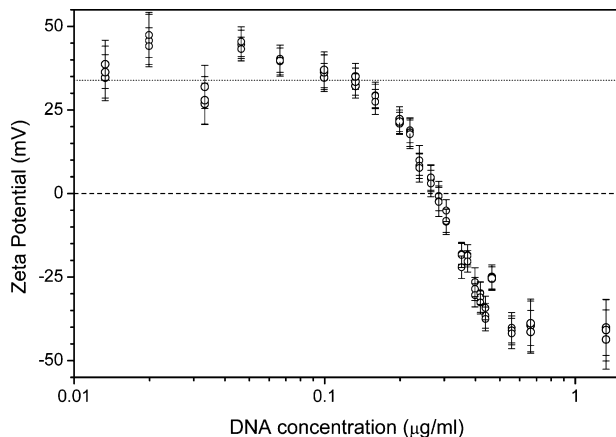
Fig. 5. The zeta potential as a function of DNA concentration for 250 bp DNA complexed with 60 nm radius spheres. The dotted line indicates the measured value for bare spheres of 33.9 mV zeta potential, while the dashed line denotes the zero potential.

Complexes formed from 60 nm radius spheres with the smaller 100 bp DNA show similar behaviour, as can be seen in Fig. 6. Again the zeta potential drops with increasing DNA concentration, but for the 100 bp DNA the concentration at which the complexes become negatively charged is lower than for the 250 bp DNA. The maximum negative zeta potential plateau is again at ~40 mV, with this value is reached at a concentration of ~0.12 μg/ml.

Unlike the zeta potential measurements on complexes with 60 nm radius spheres which all showed monomodal behaviour, indicating the presence of a single charged species in solution, complexes with the smaller 10.5 nm radius spheres showed a distinctive multimodal behaviour. Fig. 7 shows this phenomenon for complexes of 10.5 nm radius spheres with 250 bp DNA.

The dominant mode in the zeta potential measurements follows similar behaviour to that seen in Figs. 5 and 6 for complexes with 60 nm radius spheres. The secondary mode decreases in amplitude as the DNA concentration is increased, and it corresponds to a zeta potential on the order of that measured for the

Fig. 7. Zeta potential as a function of DNA concentration for 250 bp DNA complexed with 10.5 nm radius spheres. The dotted line indicates the measured value for bare spheres of 87.8 mV zeta potential, while the dashed line denotes the zero potential. Filled symbols indicate the dominant mode, while open symbols indicate other modes; the relative amplitudes of these modes are shown in the inset.

bare spheres. This mode therefore appears to correspond to free uncomplexed spheres in solution. As the DNA concentration is increased, free spheres become incorporated into complexes and the mode disappears. Similar behaviour for 10.5 nm radius spheres with 100 bp DNA is shown in Fig. 8.

At the highest DNA concentrations shown in Fig. 8, the distribution becomes multimodal (immediately after the complexes become overcharged, the distribution is monomodal). This behaviour is likely to correspond to an excess of DNA in solution due to saturation of the complexes.

Each of the four DNA/sphere complexes studied displays a similar pattern of behaviour. As can be seen from the dynamic light scattering data presented in Figs. 1–4, complexes are stable at low and high DNA concentrations and show a peak in the measured hydrodynamic radius over a critical intermediate concentration range corresponding to the presence of large
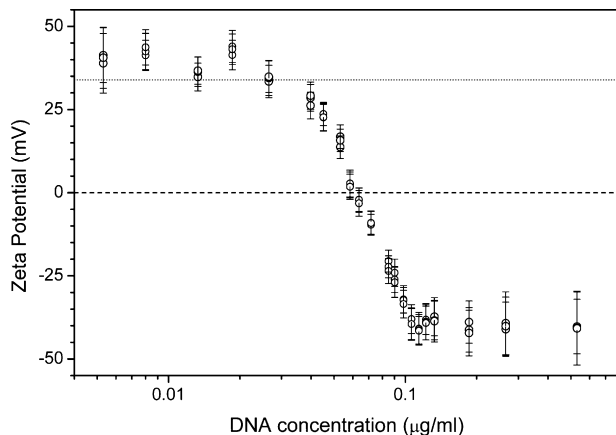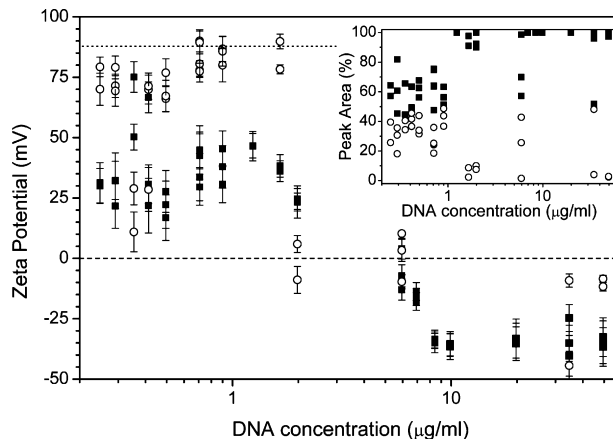

Fig. 6. The zeta potential as a function of DNA concentration for 100 bp DNA complexed with 60 nm radius spheres. The dotted line indicates the measured value for bare spheres of 33.9 mV zeta potential, while the dashed line denotes the zero potential.

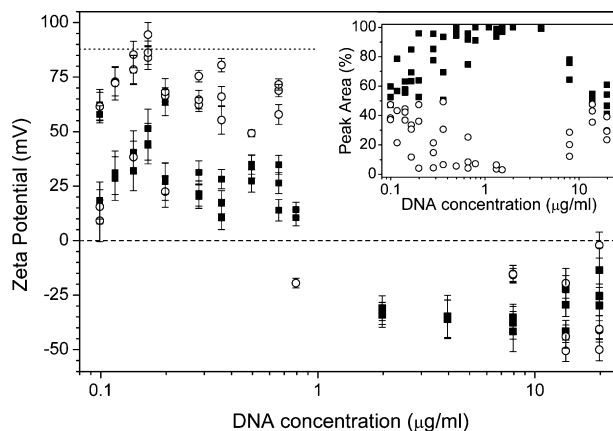Fig. 8. The zeta potential as a function of DNA concentration for 100 bp DNA complexed with 10.5 nm radius spheres. The dotted line indicates the measured value for bare spheres of 87.8 mV zeta potential, while the dashed line denoted zero potential. Filled symbols indicate the dominant mode, while open symbols indicate other modes; the relative amplitudes of these modes are shown in the inset.

aggregates in solution, which for some samples were so massive that they precipitated out of solution. For the larger 60 nm radius spheres, the radii of the complexes in the two stable regions were similar to those measured for the bare spheres, suggesting that both *over* and *under charged* complexes were formed from a single sphere with an adsorbed layer of DNA (Figs. 1 and 2). This is not the case for the smaller 10.5 nm radius spheres, which have radii similar to that measured for the bare spheres at low DNA concentrations in the *undercharged* regime, but significantly larger radii (by a factor of at least 2) in the stable *overcharged* region at higher DNA concentrations. This implies that these high DNA concentration complexes are formed from a number of spheres held together by DNA, while at low DNA concentrations the complexes consist of a single sphere with a compact adsorbed layer as in the case of the larger spheres.

The zeta potential measurements presented in Figs. 5–8 allow an explanation for the stable and unstable complexes seen in the DLS experiments to be created. All four sets of data display a similarly shaped curve. At low concentrations in the *undercharged* regime the measured zeta potential is positive, and as the DNA concentration is increased, the zeta potential becomes less positive until at a critical concentration it reaches zero. As the DNA concentration is increased further, the zeta potential becomes negative, until a maximum negative potential is reached, at concentrations beyond which the zeta potential remains constant in the *overcharged* regime. At low concentrations of DNA, the positive zeta potential indicates that the complexes have a net positive charge, and are stabilised in solution by their repulsive behaviour. The complexes are again stabilized by repulsive behaviour at high DNA concentrations, but now this is due to the complexes having a negative zeta potential. This negative zeta potential stems from the spheres adsorbing an excess amount of DNA, resulting in a complex with net negative charge [17]. The range of concentrations where large aggregates were seen to form in the DLS experiments corresponds to the crossover between positive and negative zeta potentials. At zeta potentials close to zero, neutral complexes are formed which are unstable due to the absence of electrostatic repulsion between them, and can approach each other more closely and aggregate.

By examining Figs. 1–8, it was possible to determine the DNA concentration required for the formation of neutral complexes. The concentrations found are presented in Table 1.

Table 1
Experimentally determined concentrations of DNA required for the formation of neutral complexes

DNA size (base pairs)	Sphere radius (nm)	c_{DNA} from DLS (μg/ml)	c_{DNA} from zeta potential (μg/ml)
250	60	0.33	0.28
100	60	0.079	0.060
250	10.5	6.9	4.5
100	10.5	1.35	1.2

For 60 nm radius spheres these values apply for a sphere concentration of 25 μg/ml, and for 10.5 nm radius they apply for a sphere concentration of 100 μg/ml.

Table 2
Theoretical concentrations of DNA required to neutralise 60 nm radius spheres at 25 μg/ml and 10.5 nm radius spheres at 100 μg/ml

Sphere radius (nm)	Number of charge groups per sphere[a]	Number of base pairs required	c_{DNA} (μg/ml)
60	23,000	46,000	1.2
10.5	250	500	9.9

[a] Quoted by the manufacturer.

The concentrations at which DLS samples containing 60 nm radius spheres formed neutral complexes and precipitated out of solution are shown in Table 1. The DLS samples containing 10.5 nm radius spheres aggregated across a wide range of concentrations, so the midpoint of the peak was estimated from the values at the base. The concentration required for the formation of neutral complexes in zeta potential experiments was found by estimating where the zeta potential would pass through zero following the trend of the data. It can be seen that the concentrations determined from zeta potential measurements are in all cases slightly lower than the corresponding values determined by DLS. This is likely to be due to the small quantity of added salt (5 mM NaCl) in the samples used to make zeta potential measurements.

If it is assumed that the spheres carry the full charge as determined by the manufacturer (from conductometric titration), and that the DNA is subject to Manning condensation [18] (and as a consequence carries ~25% of its bare charge), it is possible to calculate theoretical values for the DNA concentrations required to neutralise the spheres (Table 2).

Comparing Tables 1 and 2, two points become evident. Firstly, the concentrations obtained from the theoretical calculations are significantly larger than those found experimentally, and secondly, although a *single* mass concentration of DNA monomers should be required to neutralise a given size of sphere, independent of the DNA length (based on the assumptions made for the theoretical calculation), this is not seen to be true experimentally. The smaller 100 bp DNA formed neutral complexes at lower DNA concentrations than the larger 250 bp DNA.

These discrepancies suggest that the assumptions made in the calculation of the theoretical values, that the spheres carry the bare charge quoted by their manufacturer and that the DNA carries 25% of its bare charge due to Manning condensation, are inappropriate in this instance. As the theoretical calculation *overestimates* the values, this suggests that the system contains a smaller number of DNA charges than were included in the calculations, and leads to the consideration of whether the spheres are fully ionized or whether all of the absorbed DNA is available to neutralize the colloidal charge, as was assumed.

The idea of counterion condensation, and the accompanying reduction of effective charge, for a linear polyelectrolyte based on the works by Manning [18] and Oosawa [4] is well established. For a chain with a linear charge density above a critical value, counterions "condense" back onto the chain in order to reduce the "effective" charge back to the critical threshold (which is a function of the Bjerrum length). The chain with its condensed counterions then behaves as if it carries a reduced

effective charge (i.e. the combination of ionised groups on the chain plus condensed counterions) rather than the structural one (consisting solely of ionised groups on the chain).

A number of theoretical approaches to ionic condensation in spherical colloidal suspensions are discussed by Belloni [5]. It is shown that the concept of an effective colloidal charge (Q_{eff}) is widely used and often treated as an adjustable parameter. At low colloid and salt concentrations modeling the accumulation of counterions around colloids is relatively straightforward. Using the simplest mean-field theory based on the Poisson–Boltzmann equation, it can be shown that the potential around an isolated colloid results in counterions being attracted in the region of the colloid surface while co-ions are repelled. In order to determine which of these counterions can be considered condensed onto the colloid, an appropriate cut off point is identified. A condensation criterion is derived, analogous to that used for linear polyions in Manning condensation. Ionic condensation on colloids will only take place when the following inequality holds

$$\frac{Q_{geom} l_B}{4R} \geq 1 \tag{7}$$

where the counterion valency is 1, Q_{geom} is the charge on a fully dissociated colloid, l_B the Bjerrum length and R is the colloid radius. For the amidine functionalized spheres used in these experiments which have a fully dissociated charge (Q_{geom}) of +23,000e and +250e for the 60 nm and 10.5 nm colloids respectively, the inequality is true in both cases, so charge condensation will reduce the effective colloidal charge.

Evidence of counterions condensing onto charged spheres has been previously observed experimentally. Huang et al. [6] studied the electrophoretic mobility of carboxyl terminated dendrimers as a function of pH and ionic strength. Their largest dendrimers (generation five) had a lower surface charge density than their smallest dendrimers (generation two) despite the structural charges (Q_{geom}) being −972e and −36e respectively, which they conclude is a result of counterion binding. The electrophoretic mobility measured for their smallest dendrimer exceeded that for the largest dendrimer, contrary to expectations, as the latter had a significantly higher surface charge density. This led Huang to consider effective surface charge densities lower than the geometrical surface charge density. This same behaviour is seen for the amidine spheres studied in the present work.

As can be seen in Table 1, the amount of DNA required to neutralize the spheres is dependent upon the DNA size. As the amount of counterion condensation onto the sphere should be invariant with DNA length, this suggests that the shorter DNA is more effective at neutralizing the sphere's charge. This is likely a result of more efficient packing by the shorter DNA. Indeed preliminary measurements with long plasmid (3400) DNA show similar trends to that of 250 bp herring DNA, i.e. multi-sphere overcharged aggregates induced by a strong polyelectrolyte bridging interaction.

The small increases in hydrodynamic radius with increasing DNA concentration at low DNA concentrations suggest that the adsorbed layer is relatively compact. This is in agreement with the theory presented by Schiessel [19], who considers phase diagrams for complexes of a single sphere (of fixed radius) with an oppositely charged chain (of varying length). The phase diagram is plotted as a function of L_p/μ, where L_p is the persistence length of the chain and μ is the attraction between the sphere and an associated loop of chain (which is a function of the Bjerrum length, the sphere charge and the separation between charges on the chain). When L_p/μ is less than the sphere radius (R) the chain is tightly wrapped onto the sphere surface, while above this value the chain forms loops and only contacts the sphere along finite lengths of chain. The inequality holds true in all the cases studied implying the chains are tightly wrapped on to the spheres with no loops.

If the adsorbed DNA formed a single layer on the surface of the sphere, then this would give a very small increase in radius, as the thickness of a DNA chain is only 2 nm. Although the increases in hydrodynamic radius with DNA concentration seen in Figs. 1–4 are small, they are visible in all cases. Walker and Grant [20] studied the adsorption of several sizes of monodisperse single stranded DNA (oligonucleotides) onto the same 60 nm radius spheres used in this study. Their zeta potential measurements showed similar behaviour to Figs. 5–8, with the concentration for the formation of neutral complexes being lower than that calculated theoretically. However, in contrast to our results, their zeta potential curves collapsed onto a master curve when plotted as a function of DNA mass concentration, indicating that their ssDNA samples were all of a similar linear charge density [17] and the size of their flexible single stranded DNA chains did not affect the morphology of the resultant complexes. Furthermore photon correlation spectroscopy experiments were unable to determine the thickness of their adsorbed layer, as it was sufficiently small to lie within the uncertainty of the bare sphere measurement. They describe a possible "zippering" mechanism by which the DNA is adsorbed onto the surface in a compact conformation. A DNA molecule forms one or more contact points with an oppositely charged sphere, the segments of the chain adjacent to these contact points are then pulled down onto the surface. In this way the entire chain is adsorbed onto the surface, with the region of contact growing outwards from the initial point. As the regions where the DNA has already adsorbed onto the surface will have unfavorable adsorption energies compared to DNA free regions, the layer contains few cross-over points, and has a small thickness. As the system studied in the current work utilizes double stranded DNA, which is significantly more rigid than single stranded DNA, it is possible that although the majority of the chains are adsorbed onto the surface in a flat conformation, chain ends stick out into the solution, giving the sphere a slightly hairy surface layer and leading to the increase in hydrodynamic radius seen in the data. This is increasingly likely in the overcharged region, where the DNA is more closely packed, driven by correlations between the molecules forming the adsorbed layer [17]. In Schiessel's phase diagrams [19], when the length of polymer used is greater than the isoelectric wrapping length (i.e. the length of chain required to exactly neutralize the sphere) the excess chain forms a tail in solution. As the maximum amount of DNA that can be adsorbed onto a sphere is highly unlikely to be an integer number of chains through non-sequential adsorption, it is likely that some chain

ends will be protruding into the solution. Furthermore in the current experimental study this leads to multisphere aggregates at high DNA concentrations only with the amidine spheres of smaller radius, where the dangling ends effect is more important (the persistence length is smaller than the sphere radius) and gives rise to a strong DNA bridging interaction.

The result that complexation of DNA with positively charged amidine spheres leads to large weakly or neutrally charged complexes is in qualitative agreement with the theory of Cherstvy and Winkler [13]. It contradicts the results of both Netz and co-workers [21] and Nguyen and Shklovskii [22,23] that complexes should be strongly overcharged. However, more work is required to apply quantitative theory to experiments on polyelectrolyte complexation, particularly with respect to the strength of the bridging interaction in multisphere aggregates [14].

4. Conclusions

Relatively monodisperse complexes were formed by the adsorption of duplex DNA onto the surface of amine functionalized polystyrene spheres in the limit of high and low DNA concentrations. Complexes showed three regions of behaviour with DNA concentration, with stable *under-* and *over-charged* complexes present at low and high concentrations respectively, divided by a central intermediate regime characterised by the formation of large unstable aggregates. In this central regime, the measured zeta potential was found to be around 0 mV, indicating that the aggregation was a result of the formation of unstable neutral complexes. This neutral aggregate regime was found to occur at a lower concentration than expected when compared with simple charge balance stoichometric calculations for the formation of neutral complexes for all four samples studied. Small spheres formed multiglobule overcharged complexes whereas the larger spheres formed single globule complexes in the overcharged regime. The structure of DNA/colloid complexes is thus sensitively dependent on the colloidal radius when it is of the same magnitude as the DNA persistence length. This geometrical effect can switch on or off the DNA *bridging interaction* between the colloidal spheres.

References

[1] R.P. Netz, J.F. Joanny, Macromolecules 26 (1999) 9026–9040.
[2] H. Schiessel, J. Rudnick, R. Bruinsma, W.M. Gelbart, Europhys. Lett. 2 (2000) 237–243.
[3] H. Schiessel, Macromolecules 9 (2003) 3424–3431.
[4] F. Oosawa, Polyelectrolytes, Marcel Dekker, 1971.
[5] L. Belloni, Colloids Surf. A 1 (1998) 227–243.
[6] Q.R. Huang, P.L. Dubin, C.N. Moorefield, G.R. Newkome, J. Phys. Chem. B 104 (2000) 898–904.
[7] V.S. Shenoy, I.K. Vijay, R.S.R. Murthy, J. Pharm. Pharmacol. 57 (2005) 411–421.
[8] B.M. Kinsey, C.L. Densmore, F.M. Orson, Curr. Gene Ther. 5 (2005) 181–194.
[9] A. Hardada, K. Kataoka, Y. Nagasaki, Adv. Drug Deliv. Rev. 47 (2001) 113–131.
[10] S.S. Davis, L. Illum, S. Stolnick, Curr. Opin. Colloid Interf. Sci. 1 (1996) 660–666.
[11] A.A. Zinchenko, N. Chen, J. Phys. Condens. Matter 18 (2006) R453–R480.
[12] A.A. Zinchenko, K. Yoshikawa, D. Baigl, Phys. Rev. Lett. 95 (2005) 228101.
[13] A.G. Cherstvy, R.G. Winkler, J. Chem. Phys. 125 (2006) 064904.
[14] R. Podgornik, M. Licer, Curr. Opin. Colloid Interf. Sci. 11 (2006) 273–279.
[15] W.W. Tscharnuter, Appl. Optics 24 (2001) 3995–4003.
[16] B. Chu, Laser Light Scattering, Academic Press, 1991.
[17] A.Y. Grosberg, T.T. Nguyen, B.I. Schlovskii, Rev. Modern Phys. 74 (2002) 329–345.
[18] G.S. Manning, J. Chem. Phys. 51 (1969) 924–933.
[19] H. Scheissel, J. Phys.: Condens. Matter 15 (2003) R699–R774.
[20] H.M. Walker, S.B. Grant, Colloid Surf. A 119 (1996) 229–239.
[21] J.F. Joanny, M. Castelnovo, R.P. Netz, J. Phys.: Condens. Matter 12 (2000) A1.
[22] T.T. Nguyen, B.I. Shklovskii, J. Chem. Phys. 114 (2001) 5905.
[23] T.T. Nguyen, B.I. Shklovskii, J. Chem. Phys. 115 (2001) 7298.